# Stabilization of Radical Active Species in a MOF Nanospace to Exploit Unique Reaction Pathways

SCHOLARONE™
Manuscripts

# COMMUNICATION

## Stabilization of Radical Active Species in a MOF Nanospace to Exploit Unique Reaction Pathways

Yuki Harada,[a] Shinpei Kusaka,[a] Toshinobu Nakajo,[a] Jun Kumagai,[b] Cho Rong Kim,[a] Joo Young Shim,[a] Akihiro Hori,[a] Yunsheng Ma,[a,c] Ryotaro Matsuda *[a]

**We synthesized a metal–organic framework (MOF) using a ligand bearing haloalkoxy chains as a radical precursor. The radicals generated in the MOF upon photoirradiation were stable even at 250 K or under an $O_2$ atmosphere, despite radicals generated from the ligand decomposing at 200 K; thus, the regular arrangement of radicals effectively stabilized them. Moreover, a unique photoproduct was obtained only in the MOF, indicating that the confinement effect in the nanospace enabled a specific reaction that did not occur in the bulk state. We propose a new platform for exploring chemical reactions and materials based on reactive species.**

Controlling chemical reactivity using nanospace materials is an active research area.[1,2] Molecules trapped in nanospaces are strongly influenced by the size, shape, and electrostatic field of the nanospace and can be fixed in specific configurations, orientations, and arrangements.[3-6] Thus, reactions with high yields or selectivity—and, in some cases, reactions unique to nanospaces—can be observed.[7,8] Therefore, the development of nanospace materials is emerging an important research topic in reaction chemistry.

Metal–organic frameworks (MOFs) have recently attracted attention as a new class of nanospace materials.[9-11] MOFs are crystalline solids constructed using various metal ions and organic ligands, which can be periodically and regularly arranged in the framework.[12-14] For example, the introduction of metal ions or organic ligands with catalytic moieties as a building block in MOFs has been reported to lead to higher yields and selectivity of alcohol oxidation[15,16] or coupling reactions[17,18] compared with the corresponding reactions in solution. However, in recent years, new research toward using nanospaces to stabilize highly reactive species that are quickly deactivated in the bulk state has emerged.[19] With the proper arrangement of the active species in the MOF nanospace, the distance between them can be kept sufficiently large, preventing deactivation of the active species. For example, we generated a triplet carbene by photoirradiation to an azide-functionalized MOF and found that it remained stable at a temperature 70 K higher than the carbene generated from organic ligand.[20] Such a method in which stable precursors are introduced into MOFs in advance and converted into active species under external stimuli (i.e., the so-called post-synthetic modification (PSM) method) is useful for introducing active species into MOFs.[21,22]

In the present research, we focused on radicals as active species. Radical species are important in various fields of chemistry, physics, biology, and medical science.[23,24] Molecules with radicals and an open-shell structure have unique magnetic,[25] electronic,[26] and/or optical properties[27] and can be used as catalysts or organic magnets[28] and in spin-labeling.[29] However, radicals generally exhibit short lifetimes, especially at room temperature or under an $O_2$ atmosphere, because of their high reactivity. Therefore, kinetic or thermal stabilization of
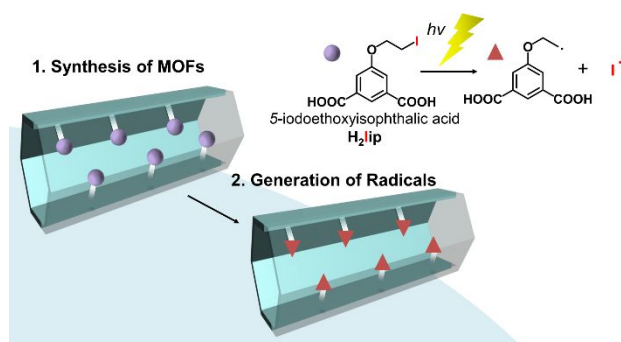


**Fig. 1** Stabilization of radicals by arrangement in an MOF nanospace using the PSM method.

[a.] Department of Chemistry and Biotechnology, School of Engineering, Nagoya University, Chikusa-ku, Nagoya 464-8603, Japan.
[b.] Institute of Materials and Systems for Sustainability, Division of Materials Research, Nagoya University, Chikusa-ku, Nagoya 464-8603, Japan.
[c.] School of Chemistry and Materials Engineering, Jiangsu Key Laboratory of Advanced Functional Materials, Changshu Institute of Technology, Changshu, Jiangsu 215500, PR China.

radicals is necessary to facilitate their handling. Currently, steric protection with bulky substituents and electron delocalization with wide π-conjugated molecules are the most popular approaches to radical stabilization.[30,31] However, such radical stabilization methods using special substituents often lead to problems such as complicated syntheses and a loss of radical activity. Therefore, we speculated that we could easily stabilize radicals with high activity by regularly arranging and isolating them in an MOF nanospace. Such radicals will lead to making new materials for selective gas adsorption and solid-phase catalysis based on the strong chemical interactions of radicals.

We synthesized an MOF using optically transparent $Zn^{2+}$ ions and organic ligands with haloalkoxy chains as precursors of radical species (Fig. 1). After photoirradiation to the MOF, we observed a radical species and found that it was chemically and thermally more stable than the species generated in the original ligand solid. In addition, we observed a unique reaction in the MOF that was not observed in the bulk state.

Upon photoirradiation, iodoalkanes are known to generate alkyl and iodo radicals via homolytic C–I bond dissociation. Therefore, we designed and synthesized 5-(2-iodoethoxy)isophthalic acid ($H_2$Iip) as a MOF building block (the synthesis procedures are shown in Supporting Information, Figs. S1 and S2). $H_2$Iip has an iodoalkoxy chain as a radical precursor and two carboxylate groups as moieties that coordinate to metal ions. We photoirradiated $H_2$Iip powder under a He atmosphere at 80 K and monitored the formation of radicals by collecting an electron-spin resonance (ESR) spectrum. Upon photoirradiation to $H_2$Iip, four sharp peaks appeared between 324 and 327 mT, which are typical of organic radicals, whereas no signal was observed before photoirradiation (Fig. 2(a)). These signals increased in intensity with increasing irradiation time, indicating that radicals were generated by the photoirradiation.

Then, we evaluated the thermal stability of the radicals generated in $H_2$Iip. After the photoirradiation was stopped, the
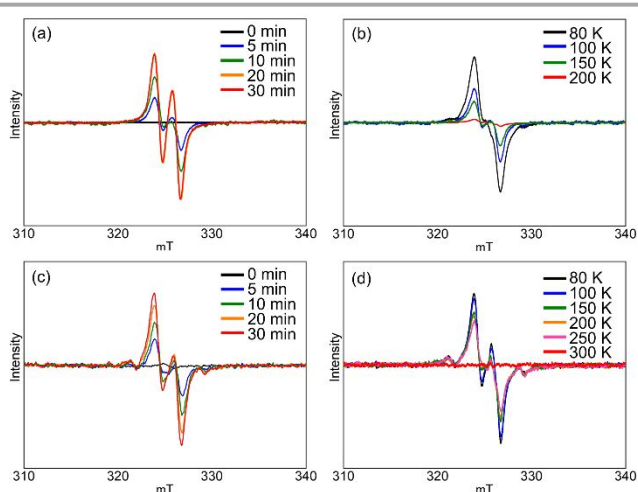


**Fig. 2** The ESR spectra of (a), (b) $H_2$Iip; (c), (d) **ZnIip**. (a), (c) Spectral change with increasing photoirradiation time. (b), (d) Spectra acquired at 80 K after heating at the attained temperatures.
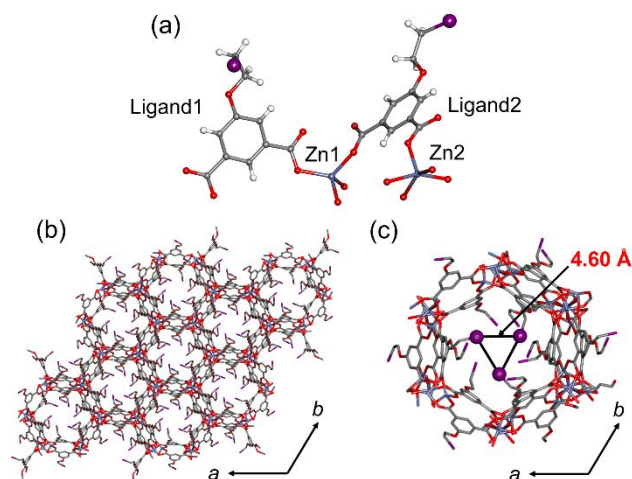


**Fig. 3** Crystal structure of **ZnIip**: (a) asymmetric unit and (b) honeycomb network structure; (c) an enlarged view of the nanopore (white, H; gray, C; red, O; purple, I; dark-blue, Zn). In (b) and (c), hydrogen atoms are omitted for clarity.

temperature was increased from 80 to 100 K at 10 K/min, maintained at 100 K for 10 min, and then lowered to 80 K for acquisition of the ESR spectrum. This process was repeated using higher temperatures (150 and 200 K). The intensity of the radical peaks gradually decreased when the heating was repeated, and the peaks almost disappeared at 200 K, indicating that ~200 K was the limit at which the radicals could exist (Fig. 2(b)).

To characterize the photoproduct, we recorded the nuclear magnetic resonance (NMR) spectrum of the photoirradiated sample (see Fig. S3 for the sample preparation) which was dissolved in DMSO-$d_6$. The NMR spectrum indicated that 5-hydroxyisophthalic acid was produced, which was confirmed by the authentic sample prepared separately (Figs. S4-S7). We calculated the conversion ratio to be 19% by comparing the integrated peak area with that in the spectrum of unreacted $H_2$Iip.

We next prepared a single crystal of $[Zn_2(Iip)_2(H_2O)]$ (**ZnIip**) by heating zinc acetate dihydrate and $H_2$Iip in a water/MeOH solution at 50 °C for 3 days. Single-crystal structural analysis revealed two crystallographically independent Iip ligands and $Zn^{2+}$ ions (Fig. 3(a), Table S1). Six ligands are linked with six $Zn^{2+}$ ions to form six-membered rings, which are linked with each other to form a honeycomb three-dimensional framework with a one-dimensional pore. The iodoalkoxyl chains are exposed inside the pores (Fig. 3(b)). The distance between nearest-neighbor I atoms is ~4.6 Å (considering the disordered I atoms), indicating that each side chain is well separated to avoid molecular collision (Fig. 3(c)). We thus reasonably assumed that generated radicals at the end of chains did not react with each other in the pore. The smallest cross-section size of the one-dimensional channel is estimated to be 1.4 × 1.4 Å², which is too small for guest molecules to access the interior pores. If all of the I atoms are removed by the photoirradiation, the pore size could increase to 6.3 × 6.3 Å². Thermogravimetric (TG) analysis showed that **ZnIip** is thermally stable to at least 423 K, with the loss of the crystal solvent molecules (Fig. S8).
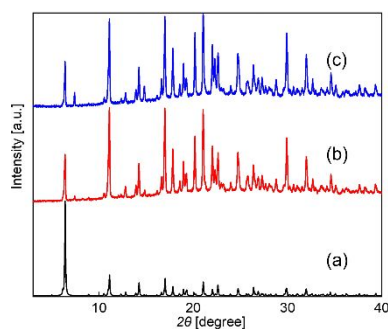
**Journal Name**

**COMMUNICATION**



**Fig. 4** PXRD patterns of **Znlip**. (a) simulation (b) as-synthesized, (c) after photoirradiation.

We subsequently photoirradiated **Znlip** activated at 393 K and monitored the generation of radicals by ESR measurements using the same procedure previously described for the H$_2$lip powder. The resultant spectra showed ESR signals similar to those of H$_2$lip, and the peak intensity increased with increasing irradiation time (Fig. 2(c)). Notably, however, two additional signals were observed at 321 and 328 mT, which were not observed in the ESR spectrum of photoirradiated H$_2$lip, indicating that different radical was generated in the MOF nanospace. In addition, we found that the thermal stability of the radicals in the MOF nanospace was enhanced compared with that of the radicals in the ligand powder. As previously noted, the radical peak intensity in the ESR spectrum of photoirradiated H$_2$lip was diminished after the sample was heated at 200 K; however, that of photoirradiated **Znlip** was clearly maintained even after the sample was heated at 250 K (Fig. 2(d)).

We characterized the structure of the photoirradiated **Znlip** using powder X-ray diffraction (PXRD). The PXRD patterns before and after photoirradiation were similar, indicating that the framework was maintained (Fig. 4). Elemental analysis of the sample was carried out by scanning electron microscopy (SEM) in conjunction with energy-dispersive X-ray spectroscopy (EDX). The I/Zn elemental ratio was determined to be ~1.0 before photoirradiation (49 at% I, 51 at% Zn), consistent with the crystal structure of the sample. After photoirradiation, the ratio decreased to 0.79 (44 at% I, 56 at% Zn), suggesting that radicals were generated by C–I bond cleavage and that the resultant I$_2$ or iodide molecules were removed from the pores during the heating process (Fig. S9). To our surprise, the $^1$H NMR spectrum of photoirradiated **Znlip** (see Fig. S3 for the sample preparation) digested in DMSO-$d_6$ showed that not only 5-

hydroxyisophthalic acid but also 5-(ethenyloxy)isophthalic acid, which was not observed in the spectrum of photoirradiated H$_2$lip, was produced, with conversion ratios of 22% for 5-hydroxyisophthalic acid and 11% for 5-(ethenyloxy)isophthalic acid, respectively (Figs. S10 and S11). The reaction ratio was 1.7 times greater than that achieved with H$_2$lip, indicating that the regular arrangement of organic ligands in the MOF pores suppressed the deactivation of the radicals. The yields of photoproduct were 19% and 33% for H$_2$lip and **Znlip**, respectively, which were higher than those estimated from the reaction on the surface of the particles (2.9-7.3%; accounting for the particle size of 200-500 nm), indicating that the reaction occurred inside the crystals.

We also investigated the difference in durability against O$_2$ between radicals generated by the photoirradiation to H$_2$lip and those in the nanospace of **Znlip**. After radicals were generated in both H$_2$lip and **Znlip** by photoirradiation at 80 K, the temperature was increased to 90 K. Then, 1 atm of O$_2$ was introduced into the sample cell and the radicals in each sample were monitored using *in situ* ESR measurements. The intensity of the radical signals in the ESR spectra of H$_2$lip rapidly decreased after the introduction of O$_2$ (Fig. S12(a)), indicating that O$_2$ directly interacted with the radicals and quenched them. By contrast, in the case of **Znlip**, the intensity of the radical signals was maintained even 300 min after O$_2$ was introduced (Fig. S12(b)), indicating that the radical species was isolated in the nanospace of **Znlip**. Because the nanospace is highly crowded with alkyl chains, the diffusion rate of molecules into the interior of the nanospace is assumed to be very low, consistent with a small amount of O$_2$ adsorption, as shown in the adsorption isotherm (Fig. S13). These results indicate that radicals were thermally and chemically stabilized in the MOF nanospace.

A plausible formation mechanism of the products under photoirradiation is shown in Fig. 5. First, alkyl radicals and iodine radicals were generated by homolytic dissociation of C–I bonds under photoirradiation. In H$_2$lip, the generated alkyl radicals were short-lived because iodine radicals remained in the vicinity of the alkyl radicals and many of them immediately recombined with the original alkyl iodide. Some of the alkyl radicals were irreversibly converted to phenoxy radicals by intramolecular β-cleavage and ethylene elimination and were finally quenched to yield 5-hydroxyisophthalic acid. We also estimated the formation energy of a phenoxy radical and an ethylene molecule from an alkyl radical using density functional theory (DFT) calculations. The calculated formation energy is very low
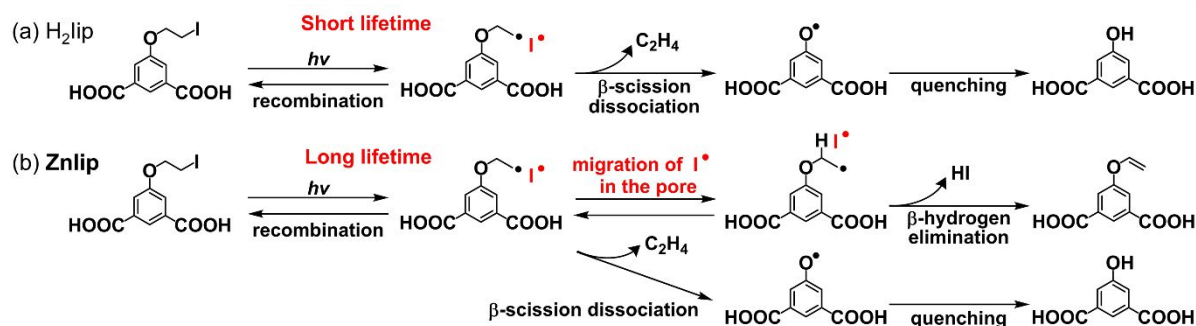


**Fig. 5** A plausible formation mechanism of the products after photoirradiation of (a) H$_2$lip and (b) **Znlip**.

(+0.51 kJ/mol), suggesting that this reaction can proceed easily via the proposed mechanism (Figs. S14 and S15). However, in **ZnIip**, the generated iodine radicals are expected to move freely in the nanopore. Therefore, after the formation of the alkyl radical and the iodine radical, the iodine radical moves through the pore and leaves the vicinity of the alkyl radical, preventing their recombination. As a result, the alkyl radicals are expected to become long-lived; thus, not only 5-hydroxyisophthalic acid but also 5-(ethenyloxy)isophthalic acid were produced via β-hydrogen elimination via attack by iodine radicals. The proposed reaction mechanism is also supported by the ESR spectrum simulation: Two distinct peaks at 321 and 328 mT which were observed only in the ESR spectrum of photoirradiated **ZnIip** (Figs. S16 and S17) are well consistent with the simulated spectrum of the alkyl radical. These results demonstrate that the nanospace can extend the lifetime of reaction intermediates that are usually short-lived and direct the reaction pathway to give products that cannot be obtained in the bulk state.

In summary, we synthesized the MOF **ZnIip** using a ligand with iodoalkoxy groups as radical precursors and generated radicals in the MOF nanospace upon photoirradiation. The generated radicals were 50 K more thermally stable than those generated from H$_2$Iip. In the present study, we found that PSM method can be applied to the stabilization of radicals. In addition, the framework of **ZnIip** protects radicals against O$_2$, which normally deactivates the radical species. We expect the results of this work to contribute to the advancement of materials science involving the physical properties of active species such as magnetic materials. Moreover, alkyl radicals were generated in the MOF nanospace by photoirradiation, which were not generated from the organic ligands. Considering that an alkyl radical is an intermediate of the photoreaction, this result indicates that the confinement effect in the nanospace enables the stabilization of such intermediates that do not easily exist in the bulk state. This research is a potential milestone in the development of new reaction chemistry in MOF nanospaces through the elucidation of reaction intermediates.

## Conflicts of interest

There are no conflicts to declare.

## Notes and references

1  P. Sudarsanam, E. Peeters, E. V. Makshina, V. I. Parvulescu and B. F. Sels, *Chem. Soc. Rev.*, 2019, **48**, 2366–2421.
2  V. Pascanu, G. González Miera, A. K. Inge and B. Martín-Matute, *J. Am. Chem. Soc.*, 2019, **141**, 7223–7234.
3  K. Komatsu, M. Murata and Y. Murata, *Science*, 2005, **307**, 238–240.
4  G. Buntkowsky, H. Breitzke, A. Adamczyk, F. Roelofs, T. Emmler, E. Gedat, B. Grünberg, Y. Xu, H.-H. Limbach, I. Shenderovich, A. Vyalikh and G. Findenegg, *Phys. Chem. Chem. Phys.*, 2007, **9**, 4843–4853.
5  M. del Carmen Giménez-López, F. Moro, A. La Torre, C. J. Gómez-García, P. D. Brown, J. van Slageren and A. N. Khlobystov, *Nat. Commun.*, 2011, **2**, 407.
6  F. C. Hendriks, D. Valencia, P. C. A. Bruijnincx and B. M. Weckhuysen, *Phys. Chem. Chem. Phys.*, 2017, **19**, 1857–1867.
7  M. Yoshizawa, M. Tamura and M. Fujita, *Science*, 2006, **312**, 251–254.
8  M. Beaumont, P. Jusner, N. Gierlinger, A. W. T. King, A. Potthast, O. J. Rojas and T. Rosenau, *Nat. Commun.*, 2021, **12**, 2513.
9  A. S. Poryvaev, D. M. Polyukhov, E. Gjuzi, F. Hoffmann, M. Fröba and M. V. Fedin, *Inorg. Chem.*, 2019, **58**, 8471–8479.
10  T. B. Faust and D. M. D'Alessandro, *RSC Adv.*, 2014, **4**, 17498–17512.
11  E. A. Dolgopolova, A. M. Rice, C. R. Martin and N. B. Shustova, *Chem. Soc. Rev.*, 2018, **47**, 4710–4728.
12  S. L. Griffin and N. R. Champness, *Coord. Chem. Rev.*, 2020, **414**, 1–20.
13  W. Danowski, F. Castiglioni, A. S. Sardjan, S. Krause, L. Pfeifer, D. Roke, A. Comotti, W. R. Browne and B. L. Feringa, *J. Am. Chem. Soc.*, 2020, **142**, 9048–9056.
14  K. Uemura, S. Kitagawa, M. Kondo, K. Fukui, R. Kitaura, H.-C. Chang and T. Mizutani, *Chem. - A Eur. J.*, 2002, **8**, 3586–3600.
15  L. Li, R. Matsuda, I. Tanaka, H. Sato, P. Kanoo, H. J. Jeon, M. L. Foo, A. Wakamiya, Y. Murata and S. Kitagawa, *J. Am. Chem. Soc.*, 2014, **136**, 7543–7546.
16  J.-L. Zhuang, X.-Y. Liu, Y. Zhang, C. Wang, H.-L. Mao, J. Guo, X. Du, S.-B. Zhu, B. Ren and A. Terfort, *ACS Appl. Mater. Interfaces*, 2019, **11**, 3034–3043.
17  A. H. Chughtai, N. Ahmad, H. A. Younus, A. Laypkov and F. Verpoort, *Chem. Soc. Rev.*, 2015, **44**, 6804–6849.
18  S. Kousik and S. Velmathi, *Chem. – A Eur. J.*, 2019, **25**, 16451–16505.
19  H. Sato, R. Matsuda, K. Sugimoto, M. Takata and S. Kitagawa, *Nat. Mater.*, 2010, **9**, 661–666.
20  T. Nakajo, J. Kumagai, S. Kusaka, A. Hori, Y. Hijikata, J. Pirillo, Y. Ma and R. Matsuda, *J. Am. Chem. Soc.*, 2021, **143**, 8129–8136.
21  S. M. Cohen, *Chem. Rev.*, 2012, **112**, 970–1000.
22  J. D. Evans, C. J. Sumby and C. J. Doonan, *Chem. Soc. Rev.*, 2014, **43**, 5933–5951.
23  I. Ratera and J. Veciana, *Chem. Soc. Rev.*, 2012, **41**, 303–349.
24  T. Hirschhorn and B. R. Stockwell, *Free Radic. Biol. Med.*, 2019, **133**, 130–143.
25  G. Mínguez Espallargas and E. Coronado, *Chem. Soc. Rev.*, 2018, **47**, 533–557.
26  T. Suga, H. Ohshiro, S. Sugita, K. Oyaizu and H. Nishide, *Adv. Mater.*, 2009, **21**, 1627–1630.
27  V. Maltese, S. Cospito, A. Beneduci, B. C. De Simone, N. Russo, G. Chidichimo and R. A. J. Janssen, *Chem. - A Eur. J.*, 2016, **22**, 10179–10186.
28  D. Maspoch, D. Ruiz-Molina, K. Wurst, N. Domingo, M. Cavallini, F. Biscarini, J. Tejada, C. Rovira and J. Veciana, *Nat. Mater.*, 2003, **2**, 190–195.
29  M. M. Haugland, J. E. Lovett and E. A. Anderson, *Chem. Soc. Rev.*, 2018, **47**, 668–680.
30  B. Tang, J. Zhao, J.-F. Xu and X. Zhang, *Chem. Sci.*, 2020, **11**, 1192–1204.
31  M. Ballester, *Acc. Chem. Res.*, 1985, **18**, 380–387.